Flexible Biradicals in Liquid and Supercritical Carbon Dioxide: The Exchange Interaction, the Chain Dynamics, and a Comparison with Conventional Solvents

Malcolm D. E. Forbes,* Katerina E. Dukes, Nikolai I. Avdievich, Elizabeth J. Harbron, and Joseph M. DeSimone

Department of Chemistry, CB No. 3290, University of North Carolina, Chapel Hill, North Carolina 27599

Received: June 13, 2005; In Final Form: November 1, 2005

X-band time-resolved electron paramagnetic resonance (TREPR) spectra of three flexible biradicals of varying chain length and structure were obtained in liquid and supercritical carbon dioxide (CO_2) solutions and compared to conventional solvents. For C_{16} acyl−alkyl biradical **1a**, an average spin exchange interaction between the radical centers, J_{avg}, was obtained by spectral simulation using a simple model for spin-correlated radical pairs (SCRPs) and a small amount of T_2 relaxation from a previously established *J* modulation mechanism. A large solvent effect on J_{avg} was observed for the first time, varying by almost 1 order of magnitude from CO_2 ($J_{avg} = -120 \pm 10$ MHz) to heavy mineral oil (-11 ± 3 MHz) for **1a**. For C_{15} bis(alkyl) biradical **1b**, spectra obtained under supercritical conditions are only slightly different from those detected in liquid CO_2 but differ from spectra taken in benzene. For C_{10} acyl−alkyl biradical **2a**, more emissive spin polarization due to $S-T^-$ mixing is observed in CO_2 than in benzene. These results are discussed in terms of solvent properties such as dielectric constant, viscosity, and specific interactions. Both chain dynamics and changes to the equilibrium distribution of end-to-end distances can alter J_{avg} and the observed ratio of $S-T^0$ to $S-T^-$ mixing; however, faster chain dynamics is concluded to be the most likely cause of the observed effects in these systems.

Introduction

In the past two decades, carbon dioxide (CO_2), in both liquid and supercritical phases, has become a solvent of great utility in separation science,[1] integrated circuit technology,[2] and polymer synthesis.[3] Liquid CO_2 is a low dielectric constant (1.2−1.5), low viscosity (∼0.05 cP at room temperature) solvent with a pressure-tunable density and easily accessible critical temperature (31 °C) and pressure (∼74 bar).[4] Many free radical reactions are possible in CO_2,[5] yet little is known about the magnetic, kinetic, and dynamic properties of free radicals or other reactive intermediates in this unusual solvent.[6] Electron paramagnetic resonance (EPR) spectroscopy is ideal for such studies, and EPR spectroscopy at high pressures presents significant experimental challenges that have been overcome in recent years.[7] In our laboratory we have constructed a high-pressure flow apparatus for the real time detection of radicals and biradicals produced during photochemical reactions in CO_2.[8]

We have had a long-standing interest in the physical and chemical properties of flexible biradicals.[9] In particular, we have studied the average exchange interaction, J_{avg}, in polymethlyene chain biradicals as a function of molecular structure,[10] magnetic field,[11] solvent,[12] and temperature.[13] In these studies, we paid particular attention to changes in the end-to-end distance distributions (a static or equilibrium property) and the rate of re-encounter of the radical centers (a kinetic property). Which of these two parameters is affected more by solvent properties is at present still subject to some debate.[12] The influence of solvent on biradical chain dynamics is therefore of continued interest, and the low viscosity and other tunable properties of CO_2 at room temperature make it an attractive solvent for such studies.

Biradicals have a long history of exploration by steady-state EPR spectroscopy, notably bis(nitroxide) structures,[14] which can have flexible spacers between the radical centers. Semiquinone-based systems have also been extensively studied, but these have typically been rigid systems in which stereoelectronic effects were the focus of attention.[15] Solvent effects are in fact rarely observed in stable biradicals, even in flexible systems. A particular disadvantage of stable systems is that once J_{avg} becomes larger than the hyperfine coupling constant (∼45 MHz for nitroxide radicals), their EPR spectra become insensitive to the magnitude of the exchange interaction. Also, such spectra are completely insensitive to the sign of J_{avg} at any magnitude.

There are therefore special advantages to studying flexible transient biradicals as carried out in our laboratory using time-resolved EPR spectroscopy (TREPR).[16] Our spectra are collected without the use of field modulation, that is, using direct detection. This is done to detect transient species present for less than 1 μs in solution at room temperature. The experiment is successful because mixing between the singlet and triplet spin states in the biradical leads to strong chemically induced electron spin polarization (CIDEP).[17] By signal averaging using a boxcar integrator and taking advantage of the CIDEP enhancements, we can retrieve almost all the signal-to-noise ratio lost by removing the field modulation. The CIDEP polarization pattern of a transient biradical carries rich mechanistic, kinetic, and magnetic information. Several research groups have devoted much of their research effort during that past two decades to careful analysis of what is known as spin-correlated radical pair (SCRP) polarization in these spectra.[18]

In this paper, we report the TREPR observation of flexible biradicals in liquid and supercritical CO_2 as compared to conventional solvents. Flexible acyl−alkyl biradicals of different

* Corresponding author. E-mail: mdef@unc.edu.

10.1021/jp053183q CCC: $33.50
Published on Web 01/13/2006

SCHEME 1

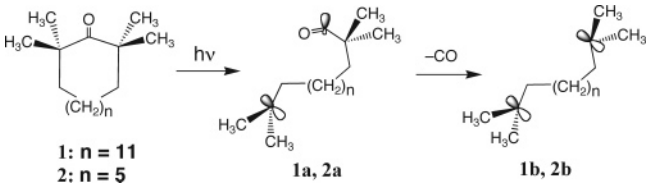

chain length were produced photochemically in CO_2, benzene, and other solvents, as outlined in Scheme 1. Laser flash photolysis of tetramethyl cyclic ketone **1** leads to Norrish I α cleavage from the first excited triplet state of the carbonyl moiety. This process initially gives biradical **1a**, a C_{16} acyl−alkyl biradical, which decarbonylates on the submicrosecond time scale to give C_{15} bis(alkyl) biradical **1b**. Ketone **2** photolyzes in a similar manner to give C_{10} acyl−alkyl biradical **2a** and decarbonylates to give bis(alkyl) biradical **2b**. Below we will show that indeed significant solvent effects are observed on the TREPR spectra of these structures with large changes in both static and dynamic biradical physical parameters observed in liquid CO_2.

Experimental Section

Our TREPR apparatus has been described in detail previously,[18a] and our modifications for high pressure are detailed in a separate publication.[8] Briefly, spectra were recorded on a Varian E-line X-band (9.5 GHz) EPR console and bridge modified with a fast preamplifier and a low noise GaAs FET microwave amplifier (25 dB gain). The microwave power incident on the samples was 10 mW for all experiments. High-pressure CO_2 solutions were circulated through a quartz flow cell of 9 mm outside diameter and 2 mm inside diameter using a specially modified micropump with a sapphire shaft. The quartz sample tube was epoxied to stainless steel pressurizing heads and centered in a home-built brass cylindrical TE_{011} microwave cavity equipped with a slotted window for light access.

The flow system included a 20 mL stainless steel reservoir with a sapphire window and magnetic stir bar. Samples of ketone (the C_{10} parent compound is a solid) were placed in the reservoir, which was then sealed and charged with CO_2 using a hand-turned HIP pump. The solution was mixed and flowed through the entire apparatus until clear by visual inspection through the sapphire window. Solutions were irradiated by a 308 nm laser pulse (20 ns width, ∼20 mJ, repetition rate 60 Hz) from a XeCl excimer laser LPX100i (Lambda Physik). The concentration of starting material was typically 0.05−0.1 M. After accounting for the light intensity, ketone extinction coefficient, and the known quantum yield for biradical formation, we estimated biradical concentrations immediately after the laser flash to be 10^{-5} M or less. For this reason, intermolecular diffusion processes were ignored.

Spectra were collected at a fixed delay time after the laser flash using a Stanford Research Systems boxcar integrator (100 ns gates), and the external field was swept over 2−4 min. All spectra and simulations shown have a sweep width of 150 G unless otherwise noted. Because of the direct detection method employed, transitions below the baseline represent emission, while those above the baseline exhibit enhanced absorption.

The precursor cyclic ketones were purchased from Aldrich (C_{10}) or Lancaster (C_{16}) and then tetramethylated with KH/CH_3I or LDA/CH_3I. Purification was carried out by column chromatography on silica gel with hexanes as the eluent. Characterization of final products was completed by ^1H NMR and GC/MS.

Safety Note: Initial pressurization of such flow systems should always be carried out with full face protection such as a visor. We also recommend using a plexiglass safety shield around the sample cell/resonator assembly at all times when the pressure is above 1 bar. On several occasions when ramping up the pressure we have experienced shattered sample cells or failure of the epoxy seals between the quartz tube and the stainless steel pressurizing heads.

Results and Discussion

Before the presentation of experimental spectra, it is useful to summarize the salient features of biradical SCRP spectra. We do this to help explain our model for spectral simulation and to define several important physical parameters relevant to both the exchange interaction and the chain dynamics for the type of biradical shown in Scheme 1. To simulate SCRP spectra, we require line positions, intensities, phase, and width. For line width and phase, we assume Lorentzian line shapes that are either purely absorptive or purely emissive. The width is input as a single fitting parameter unless a relaxation process is present that affects each line independently. Emissive or absorptive phase is determined from population differences between the electron spin states, which are explained in Figure 1. Transition intensities depend on these population differences and the transition probabilities. The probabilities and the field position of each resonance are determined by diagonalizing the spin Hamiltonian in an appropriate high field basis. The Hamiltonian is initially written in a standard basis set taken as the direct product of the four electron spin levels (T^+, T^0, T^-, S) and the nuclear spin state sublevels, χ.

Figure 1A shows a pictorial representation of the biradical energy levels at $t = 0$, that is, immediately after creation of the biradical (a process we assume to be nonadiabatic) but before any spin state mixing has taken place. We have omitted the hyperfine splitting for clarity, but it is important to note that each nuclear sublevel χ has a similar energy level diagram associated with it that can be considered independently. The situation at time = 0 is as follows: each triplet level contains $^1/_3$ of the total electronic spin state population, and the singlet level is empty. Strictly speaking, there are slight differences in the triplet level populations when the biradical precursor is a photoexcited triplet state, but for the alkyl ketones considered here, this polarization is small compared to the SCRP spectrum and can be ignored. Figure 1B shows the populations and energy levels after the S and T^0 states have mixed. This represents the situation when J_{avg} is small compared to the hyperfine interaction, a_H.

Diagonalization of the spin Hamiltonian creates two new eigenstates, Ψ_2 and Ψ_3, which have both singlet (S) and triplet (T^0) character. Any re-encounters between radical centers in the singlet state will lead to a unit probability of reaction at van der Waals contact distance (3.5 Å for these structures). In polymethylene chain biradicals, the re-encounter rates (k_{en}) are on the order of 10^9 s^{-1} (for examples of k_{en} values and other biradical simulation parameters, see refs 9a and 9b), and because of their substantial singlet character, the states Ψ_2 and Ψ_3 are depleted very quickly when J_{avg} is small. This depletion is depicted in Figure 1C and is the origin of the unusually large spin polarization often observed in these species by TREPR. At room temperature and below, this "small J" case is typically observed in long ($\geq C_{14}$) acyl−alkyl type biradicals in conventional solvents at delay times of about 100 ns after the laser flash. It is important to note that the re-encounter rate, k_{en}, is governed by the polymethylene chain dynamics (trans to gauche

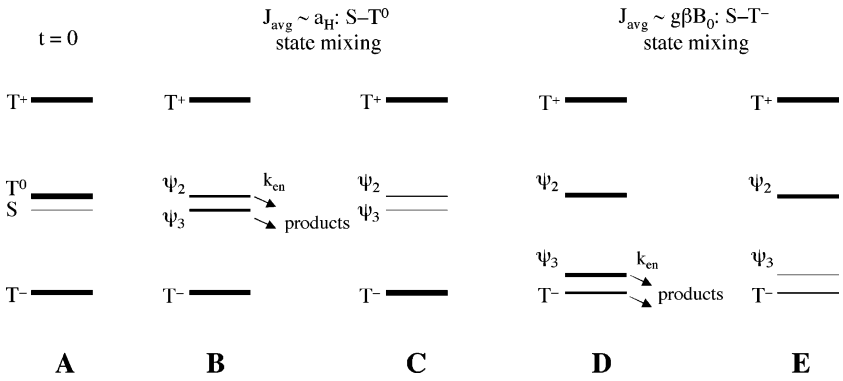

Figure 1. Electron spin state energy level diagrams for a flexible biradical created from a triplet precursor. The width of a line indicates the population of that state. Panel A shows biradical energies and populations at time = 0, that is, just after biradical creation, showing the empty singlet state and equal populations in each triplet level. The energy difference between S and T^0 is $-2J_{avg}$. In panel B, the S−T^0 mixing process creates new eigenstates, ψ_2 and ψ_3, both of which now have significant singlet character and deplete their populations by chemical reaction. The energy splitting between these states is -2ω, where $\omega^2 = a_H^2 + J_{avg}^2$. Panel C shows the resulting populations that lead to a first-order SCRP spectrum. Panel D presents the same type of diagram as that in panel B except that S−T$^-$ mixing is predominant and chemical reaction depletes both T^0 and T$^-$. Panel E shows populations that lead to a second-order SCRP spectrum with net emission from the S−T$^-$ process. See text for definitions and examples of first- and second-order spectra.

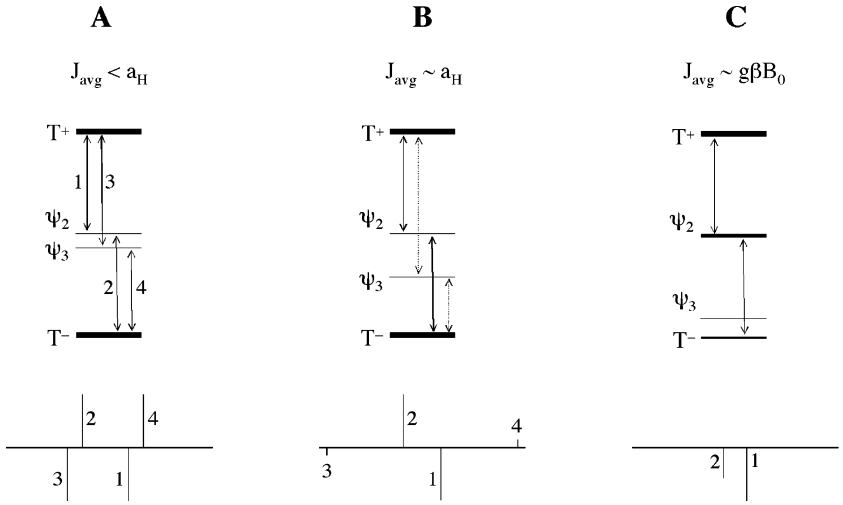

Figure 2. The top panel shows allowed transitions in SCRP spectra, labeled 1−4, and the bottom panel shows stickplots of expected EPR spectra for the case of (A) small J_{avg}, (B) $J_{avg} \approx a_H$, and (C) large J_{avg}. See text for details.

conformational transitions) and therefore, like J_{avg}, is a function of biradical chain length. We will comment further on this relationship below. It is also important to note that the time scale for encounters (1 ns) is much shorter than the time scale of observation (100−200 ns). This difference in scale is in large part the reason for the validity of the use of an average J coupling in modeling biradical TREPR spectra.

Figure 1D illustrates what happens when J_{avg} greatly exceeds the hyperfine value and becomes comparable to the Zeeman energy $g\beta\mathbf{B}_0$ (g is the electron g factor for the radical center, β is the Bohr magneton, and $\mathbf{B}_0$ is the applied external field). While S−T^0 mixing is still taking place, additional mixing between S and the T$^-$ level now becomes an important process. The predominant depletion due to chemical reaction is now from the T$^-$ level, which is shown in Figure 1E. For the biradicals discussed here, chain dynamics (i.e., k_{en} values) and J_{avg} are responsible for the interplay between the S−T^0 and S−T$^-$ mixing processes. Chemical lifetimes can be extracted from k_{en} values from the product $k_{en}\lambda_S$, where λ_S is the fraction of singlet character of the state. The λ_S values are determined from the ratio of a_H to $2J_{avg}$ for S−T^0 mixing and from the ratio of a_H to $(2J_{avg} + g\beta\mathbf{B}_0)$ for S−T$^-$ mixing.

Figure 2 shows the allowed TREPR transitions and "stickplot" spectra expected for a symmetric biradical with one hyperfine interaction, a_H. There are three important cases to be considered: (A) $J_{avg} < a_H$, (B) $J_{avg} \approx a_H$, and (C) $J_{avg} \approx g\beta\mathbf{B}_0$. The transition probabilities follow directly from spin selection rules and the ratio of J_{avg} to a_H (at large J_{avg}, two of the four transitions become more forbidden while the two others remain strongly allowed; see ref 9 for more details). For case A in Figure 2, the spectrum consists of a pair of emissive/absorptive doublets of approximately equal intensities. Apart from the anomalous phases, this spectrum is completely analogous to the AX ^{1}H NMR spectral system for two spin $^1/_2$ nuclei when $J_{AX} \ll \delta$ (where J_{AX} is the nuclear spin−spin coupling constant and δ is the nuclear chemical shift). We call this the first-order spectrum, and it is the only case in which the value of J_{avg} can be read directly off the spectrum ($2J_{avg}$ is the splitting between the absorptive and emissive component of each doublet).

Keeping in mind our NMR analogy above, we now consider what happens as J_{avg} increases in magnitude to become comparable to a_H (Figure 2B). There are still two doublets, but the splitting is so large that the outer transitions are just barely perceptible on the perimeter of the spectrum. This happens because the transition probabilities become very low when $J_{avg} \approx a_H$ (recall the "roofing" effect observed when the AX ^{1}H NMR spectrum moves to the AB spectrum as J_{AX} becomes comparable to δ). Generally the only observable transitions are

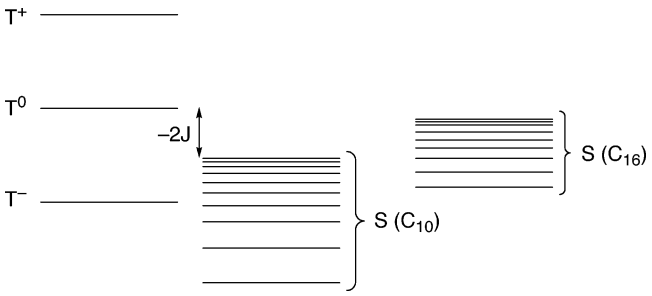

Figure 3. Energy level diagram for two flexible biradicals of chain length 16 and 10 carbon atoms at high magnetic field. In this description, the triplet energy levels (T^+, T^0, and T^-) remain fixed and separated by the Zeeman interaction, while the singlet level S is allowed to fluctuate due to chain motion. Only the smallest singlet−triplet gap is shown as 2*J*; all others are implied. Note that both the average value of 2*J* and the magnitude of the fluctuations are different for the two different chain lengths.

those labeled 1 and 2 in Figure 2B, which with increasing J_{avg} move toward the center of the spectrum to a limiting separation of $a_H/2$. In this case, the value of J_{avg} cannot be directly obtained from the spectrum but instead must be varied as a fitting parameter. This results in what we call the second-order spectrum. The state mixing process is still predominantly $S-T^0$; therefore, the line positions are still determined from the diagonalization procedure described above. However, the intensities become dependent on the ratio of $S-T^0$ to $S-T^-$ mixing and are therefore quite sensitive to J_{avg} at early delay times. At later delay times, more sensitivity to k_{en} is typically observed.

Taking this situation to the extreme where J_{avg} approaches the magnitude of the Zeeman energy, $g\beta\mathbf{B}_0$, leads to the situation outlined in Figure 2C. Only transitions 1 and 2 are observed, split exactly by $a_H/2$. Both transitions are emissive because the dominant state mixing and chemical depletion process is now $S-T^-$. The exact appearance of the spectrum in this case is complicated because the mixing process can depend on both J_{avg} and k_{en}. In general, for biradicals of the same chain length, it is mostly k_{en} that influences the amount of $S-T^-$ mixing, whereas if the chain length changes from long ($>C_{14}$) to short ($\leq C_{10}$), even for small values of k_{en}, the spectra remain emissive because J_{avg} is large. This is illustrated graphically in Figure 3 for the case of a C_{10} vs C_{16} flexible biradical. When $S-T^-$ mixing takes place, it can be a slow process (microsecond scale) to convert a second-order spectrum with equal amounts of emission and absorption into a fully emissive spectrum. This is because λ_S is often on the order of 10^{-3} or smaller in the $S-T^-$ process (λ_S is determined from the perturbation expression for the state mixing process). The depletion rate is given by the product $k_{en}\lambda_S$, so for typical re-encounter rates of 10^9 s^{-1}, recording and simulating the time dependence over about a 5 μs range can give an estimate of J_{avg} even when it greatly exceeds a_H. This is a major advantage of the TREPR method over steady-state EPR spectroscopy.

Figures 1−3 and our simulation procedure can be summarized as follows: all magnetic parameters except for J_{avg} come from the monoradical data in the literature.[9] Spin relaxation via T_1 effects (e.g., dipolar relaxation, local field fluctuations) can be included, but for biradicals observed at 100 ns, these are not important processes. An important T_2 effect is *J* modulation relaxation, but this requires knowledge of only J_{avg} and k_{en}. Line positions, intensities, and phases come directly from diagonalization of the biradical spin Hamiltonian with only J_{avg} (with the correct sign) and the line width as input parameters. The phase of the SCRP polarization tells us the sign of the *J* coupling immediately if it is previously unknown. Best fit of the line positions gives the magnitude of the coupling, and the time dependence of the signals can provide information about radical re-encounter rates, spin relaxation processes, and the magnitude of J_{avg} even when it exceeds the hyperfine value. The time dependence was not specifically addressed here because the largest changes were seen with J_{avg} and also because the decay is dominated for these structures by spin-rotation interaction induced electron spin relaxation.

An additional complication that sometimes arises in the simulation of SCRP spectra is that "ordinary" radical pair mechanism (RPM) polarization often appears as a superposition on the "pure" SCRP spectrum. Here we deal with this problem by computing the RPM pattern separately and adding it as necessary to best fit. Since both SCRP and RPM polarizations arise from the same spin physics (S−T mixing), and both are affected by radical re-encounter rates, they should be solved for simultaneously in a more rigorous approach. Our current method suffices in most cases for our biradicals, but we recognize that this procedure is not strictly correct.

More sophisticated models for the simulation of SCRP spectra have been developed by us[19] and others.[20] In the simplest model presented in Figures 1−3, called the Closs−Forbes−Norris or CFN model,[18a−b] J_{avg} and the re-encounter rate are evaluated separately, a procedure only valid under conditions of fast motion and strong exchange. This condition is largely fulfilled for the biradicals under study here. The other models, which are mostly based on solutions of the stochastic Liouville equation, incorporate interradical motion explicitly and assess the exchange interaction using a parametrized equation that is exponentially dependent on distance.[19,20] A major goal of these other models is to extract diffusion or dynamic information, but the concept of an average *J* value never appears because of the distance dependence. Instead the parameter J_0 (the value of *J* at van der Waals contact $r_0 = 3.5$ Å) is used with diffusion and distance information to fit a time-dependent TREPR dataset. Additionally, these models solve simultaneously for the RPM/SCRP superposition problem, and one paper in particular[19] addresses a special case when the kinetic and magnetic parameters combine to create a rather drastic asymmetry in the SCRP line shape. This phenomenon is not observed here and is not considered further.

At the present time, the more sophisticated simulation routines developed for the explicit incorporation of chain dynamics for both SCRP and RPM polarization patterns cannot accommodate the large line width of the biradicals studied here (~6 G at room temperature). Therefore, we proceed qualitatively with our analysis in the framework of the CFN model and note that the inclusion of *J* modulation relaxation (incorporated explicitly into the calculation for each transition using Redfield theory)[21] and RPM polarization (added as a superposition) help to give better fits to these spectra. The inclusion of *J* modulation in particular suggests that chain dynamics are important in these systems. In this situation, the outer transitions are broadened by an amount dependent on the ratio of a_H to J_{avg}. Combined with the state mixing and kinetic effects described above, the perimeter transitions can often completely disappear. The CFN model, with slight modifications, can give significant qualitative insight into both the spin exchange process and encounter rates in our biradical systems as a function of solvent.

X-band (9.5 GHz) TREPR spectra of biradicals **1a**, **1b**, and **2a** in CO_2 and in benzene are shown in Figure 4. Figure 4A shows signals from the C_{16} acyl−alkyl biradical at a 0.2 μs delay time at 298 K. These spectra were independent of pressure from

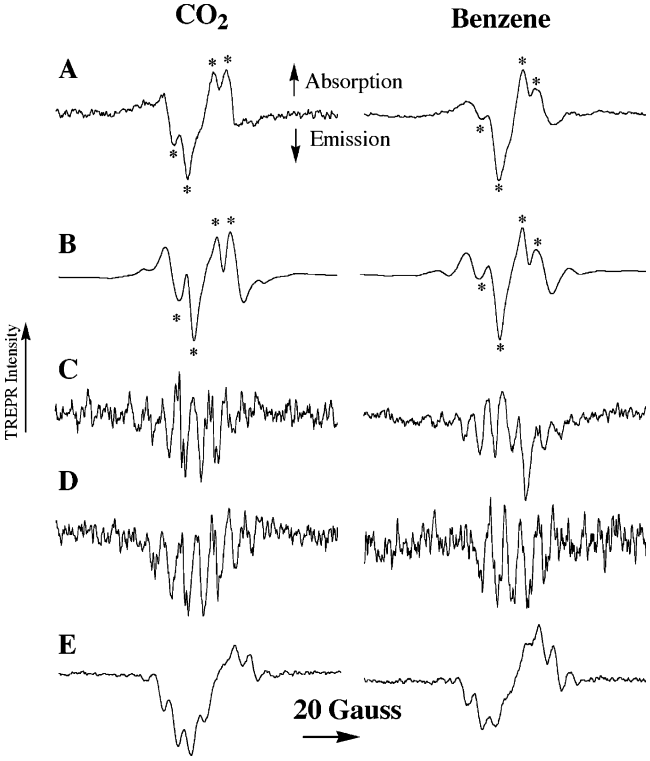

Figure 4. TREPR spectra of biradicals **1a**, **1b**, and **2a** obtained in CO_2 (left) and in benzene (right) solutions using an X-band spectrometer after a 17 ns excimer laser flash at 308 nm (~15 mJ). Spectra A show biradical **1a** at 28 °C observed at a delay time of 0.2 μs after the laser flash. Specta B are simulations of the data in spectra A. For the CO_2 spectrum, we used a J value of −120 MHz, an encounter rate (k_{en}) of 10^9 s^{-1}, and a J modulation matrix element of 100 G to fit the line widths. For the benzene spectrum simulation, J was −70 MHz, the encounter rate (k_{en}) was also 10^9 s^{-1}, and the J modulation matrix element was again 100 G. Transitions labeled with an ∗ are those most sensitive to the simulation routine using a static value for J. Other kinetic and magnetic parameters in this and all subsequent simulations are taken from previous work.[20] Spectra C show biradical **1b** at 28 °C observed at a 0.8 μs delay time. Specta D show biradical **1b** at 48 °C at 0.8 μs. Spectra E show biradical **2a** at 28 °C observed at 0.2 μs.

0.87 to 2 bar. From our previous work, we know that the transitions marked with an asterisk are those the intensities and positions of which are extremely sensitive to the magnitude of J_{avg}. Simulations of these two spectra are shown in Figure 4B. It is clear by inspection that the intensities of the indicated transitions are very different in the two solvents. The simulations are based on the CFN model,[18a] and we have included a small amount of T_2 relaxation due to J modulation,[21] which helps fit the line widths slightly better on the perimeter of the spectrum. We obtain values for J of −70 ± 10 MHz in benzene and −120 ± 10 MHz in liquid CO_2. This is the first time a significant solvent effect on J_{avg} has been observed.

At later delay times, decarbonylation of **1a** takes place to produce C_{15} bis(alkyl) biradical **1b**. The TREPR spectrum obtained at 0.8 μs delay time is shown in Figure 4C. In CO_2, the spectrum is almost completely due to biradical **1b** (see ref 9 for a comparison spectrum), but in benzene, we observe a superposition of spectra from **1a** and **1b**. This suggests that the rate of appearance of the bis(alkyl) spectrum (by decarbonylation) or the kinetics of disappearance of the acyl−alkyl spectrum (chemical reaction or spin relaxation[23]) are different in the two solvents. A solvent-dependent decarbonylation rate has been observed before in conventional solvents for radicals of similar structure,[24] as have different spin relaxation rates in acyl radical centers in different solvents.[25] When the temperature is raised to the supercritical region (>31 °C), spectra due to biradical **1b** become observable in both solvents at 0.8 μs, as shown in Figure 4D. It should be noted that the CO_2 spectrum for this biradical has more net emission due to $S-T^-$ mixing but in benzene a superposition of spectra from the two biradicals (**1a** and **1b**) still seems to be present. Acquisition of TREPR spectra in the supercritical region is hampered by poor signal-to-noise ratios, which we assume is caused by dielectric fluctuations of the sample inside the microwave resonator. Solutions of CO_2 are significantly more turbid in this region of the phase diagram.

Figure 4E shows spectra taken in liquid CO_2 and benzene for the C_{10} acyl−alkyl biradical **2a**. Here the spectrum taken in CO_2 shows a strong net emission compared to that taken in benzene. Clearly mixing between the singlet state and the middle sublevel, T^0, is overtaken by mixing with the lower sublevel, T^-. Promotion of $S-T^-$ mixing can be made possible either by a larger value of J_{avg} or by an increase in k_{en}, which causes momentary fluctuations of the end-to-end distance. This in turn leads to greater access of conformations where the instantaneous value of J is large and negative. Differences in chain dynamics between CO_2 and benzene have been reported previously for bis(alkyl) biradical **2b**,[21] where relaxation due to J modulation was observed and successfully simulated as a hyperfine-dependent alternating intensity effect. The detailed spectral analysis of **2b** in both CO_2 and benzene has been published; therefore, this structure is not considered further. It should be noted, however, that J modulation can affect line widths (T_2 relaxation) or intensities (T_1 relaxation) but rarely do both effects appear simultaneously, which is interesting and will be discussed in detail in a future publication. Qualitatively it appears that the T_2 effects appear in long biradicals when $J_{avg} \approx a_H$ and chain motion is moderate to slow and the T_1 effect is dominant in very short biradicals with fast chain motion.

CO_2 has a low viscosity (0.06 cP) at room temperature and 1 bar pressure, and its physical properties are often described as being between those of a liquid and a gas. We expect faster chain motion in the gas phase, leading to more $S-T^-$ mixing or a larger effective J value. Evidence for this has been put forward by Yurkovskaya et al.[26] in a gas-phase study of the magnetic field dependence of CIDNP in flexible biradicals. However, the fact that we used similar amounts of J modulation relaxation in our simulations from both solvents leads us to suggest that dynamics are only part of the story. If we consider the static J values to be functions of the end-to-end distance distribution of the flexible chain, a practice that has served us well in the past in analyzing biradical SCRP spectra,[9b] it is possible to interpret these data in terms of a shift in this distribution for this chain length in CO_2. Examples of such distributions, computed using a rotational isomeric state model for the polymethylene chain,[27] are shown in Figure 5 for the C_{10} and C_{16} chain lengths.

Figure 5 also shows the exponential falloff of the exchange interaction, $J(r) = J_0 \exp(-\lambda(r - r_0))$, as a function of this same distance. From these curves, a compact expression for J_{avg} can be computed (eq 1) by selecting 20−30 values of r_i and summing the products.[9b]

$$J_{avg} = \frac{\sum_i P(r_i) J_0 \exp(-\lambda(r_i - r_0))}{\sum_i P(r_i)} \quad (1)$$

Clearly a shift in the equilibrium distribution is one way to achieve a higher value for J_{avg}. However, faster dynamic

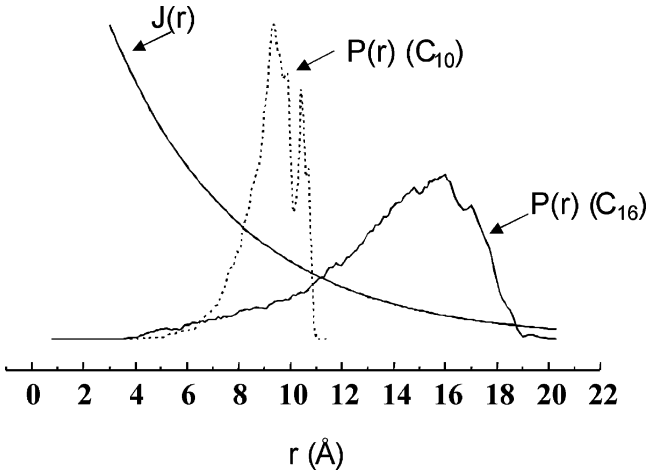

Figure 5. End-to-end distance distributions for a C_{16} and C_{10} polymethylene chain, computed using a rotational isomeric state model as per ref 27. Also shown is the exponential distance dependence of the spin exchange interaction 2*J*.

sampling of all possible distances within the same distribution can produce the same effect. The reason for this is rooted in the exponential dependence of *J*: any process that increases the sampling of shorter distances will weight the average *J* more heavily with the larger values experienced at those short distances.

It is interesting to note that there is a deep connection between the distributions shown in Figure 5 and the graphical representation of the *J* coupling shown in Figure 3 for long (C_{16}) and short (C_{10}) biradicals. The argument for this connection is as follows: jumps between different distances in the distribution plot for C_{10} lead to large changes in *J*, and fast jumping leads to a large average *J* value. For C_{16}, the *J* vs distance function is much flatter in regions of high probability. Changes in the *J* value as a function of distance are therefore much smaller for this chain length. Because of the longer distances involved, even at fast motion the average *J* value is smaller for the longer chain.

To test which of these is effects is more important, we wanted to compare J_{avg} in solvents of similar solvating ability to CO_2 but of similar viscosity to benzene. We are assuming that solvents with similar solvating abilities will have similar end-to-end distance distributions. Therefore, we have collected TREPR data at room temperature for biradical **1a** in the following solvents: methanol, acetontrile, pentane, Freon 113, and Vertrel (2,3-dihydroperfluoropentane). The latter two solvents were run because of their similar solvating properties to CO_2, while the first three were run to vary the dielectric constant over a wide range. In all of these solvents, the J_{avg} value was identical. In fact the features of the TREPR spectra (not shown) were identical in every respect: line positions, widths, intensities, and phases. The only common parameter to each of these solvents and benzene is their viscosity at room temperature, about 0.6 ± 0.2 cP.

To confirm the role of chain dynamics in these TREPR spectra, a solvent with similar polarity to benzene but a drastically different viscosity from benzene is required. In this regard, we have selected heavy mineral oil of viscosity 220 cP. If our arguments are correct, an increase in viscosity should lead to a lower J_{avg}. Figure 6 shows TREPR spectra of biradical **1a** acquired at room temperature in heavy mineral oil (Figure 6A), along with a simulation using the CFN procedure (Figure 6B). The spectrum acquired in mineral oil is at the opposite extreme of the first two solvents in that it shows a very small value of J_{avg}. This is easily seen from the spectral pattern of

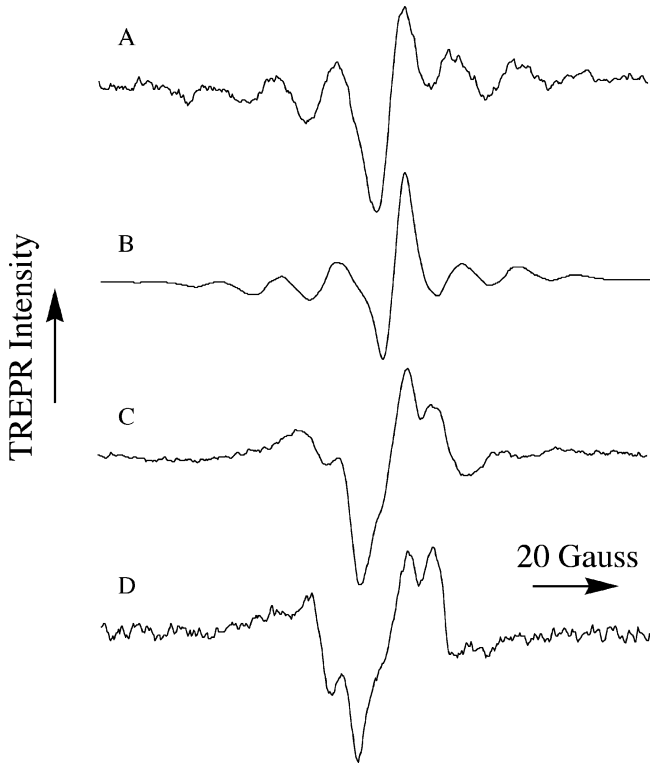

Figure 6. X-band TREPR spectra of biradical **1a** obtained in (A) mineral oil, (C) in benzene, and (D) in liquid CO_2. Spectrum B is a simulation of spectrum A using $J_{avg} = -11 \pm 3$ MHz. All spectra were acquired at 28 °C and a delay time of 0.2 μs. Note the transition from a first-order spectrum in the more viscous solvent ($J \gg a_H$) to a second-order spectrum ($J < a_H$) in CO_2.

alternating emissive and absorptive doublets, indicative of a J_{avg} value much less than the isotropic hyperfine interactions (about 50 MHz in these systems). The simulation gives $J_{avg} = -11 \pm 3$ MHz, with a small amount of RPM polarization added to best fit the slight E/A multiplet pattern superimposed on the SCRP pattern.

The spectra obtained in benzene and CO_2 are shown for comparison in Figure 6C,D, respectively. From mineral oil to CO_2, at constant temperature, J_{avg} increases by about 1 order of magnitude (the concomitant increase in viscosity is more than 4 orders of magnitude). In the mineral oil spectrum, it was not necessary to include any *J* modulation relaxation, as predicted above. The results in Figure 6, coupled with our data for other solvents for which spectra are not shown, strongly suggest that chain dynamics are the dominant parameter dictating the observed spectral pattern. The dynamics play this role by allowing faster sampling of the end-to-end distance distribution, shifting the weighted average of *J* from eq 1 to larger values. We cannot be more quantitative about k_{en} values because at about 10^9 s^{-1} the simulations become much less sensitive to this parameter, and we rely on RPM polarization, *J* modulation, and J_{avg} to dictate the spectral shape. Specific interactions, solvating ability, or shifts in the end-to-end distance distributions themselves do not seem to be major contributors to the increase in J_{avg} observed for **1a** in CO_2.

There exists the possibility of specific interactions between CO_2 and the biradical, and this is worthy of some discussion. For example, if CO_2 is a poor solvent for the biradical, then the chain segments may prefer to interact with each other rather than with the solvent,[28] thereby shifting the end-to-end distance distribution as discussed above. It is possible that the precursor ketone **1** is aggregating in CO_2 to form a microemulsion,[29] but

SCHEME 2

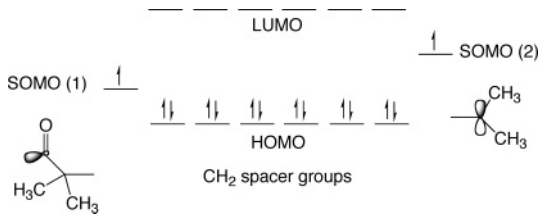

that would lead to a biradical inside an aggregate that looks very much like a hydrocarbon solvent, where we know that *J* is the same as it is in benzene. For this reason, we rule out the possibility of aggregation to the extent of microemulsions. The CO_2 could also participate directly in the coupling between the unpaired electrons, assisting in a "superexchange-type" coupling mechanism.[30] Or, there could be a specific interaction between CO_2 and the carbonyl moiety on the acyl half of the biradical. This would lower the energy of this half of the biradical, bringing the singly occupied orbital on the acyl fragment closer to the bonding orbitals of the polymethylene spacer unit, as shown in Scheme 2. This would provide better coupling to the spacer, increasing *J*.

This does not imply that the entire coupling is through-bond: the overall coupling can still be a mixture of various mechanisms (through-bond, through-space, and through-solvent), and CO_2 can assist in the coupling by interacting with just one part of the biradical (or by not interacting as well; poorer solvation leads to more coiled chains). There have been recent experimental reports of a specific interaction between CO_2 and polymers by both IR[31] and NMR[32] spectroscopies. Interactions between CO_2 and certain fluorocarbons were calculated by Cece et al.,[33] but the magnitude of these effects were later questioned.[34]

It is important to qualify this argument by stating that specific interactions should not be exclusively attributed to CO_2. One of the main reasons for its suspected high activity as a solvent has to do with the large quadrupole moment observed in this molecule. However, such a quadrupole moment exists for benzene as well. The physics of how CO_2 solublilizes organic molecules is less well-known than for benzene, but if one were to invoke a "like dissolves like" argument, CO_2 would be predicted to be the better solvent for the acyl end of the biradical than would benzene. These differences in solubilizing ability are interesting and can perhaps be studied in the future by running the TREPR experiment in mixtures of CO_2 and organic solvents, including benzene.

Summary and Outlook

We have demonstrated that large solvent effects on the spin exchange interaction in flexible biradicals can be observed if the viscosities are taken to extreme values away from conventional organic solvents. Chain dynamics, and not other specific interactions or solvent properties, are the main factor governing the observed coupling constants or the appearance of $S-T^-$ mixing. CO_2 appears to be ideal for examination of fast motion conditions, while heavy mineral oil allows investigation of the slower motion regime. Moving to much slower solvent systems such as glycerol may not provide more information because line broadening due to hyperfine and *g*-factor anisotropies may obscure the effects that we want to observe regarding the exchange interaction. Furthermore, the photochemical reaction leading to the production of the biradical in high yield may be significantly retarded in extremely viscous media due to fast geminate recombination. Our studies continue with experiments using substituents and other structural modifications on the precursors to further address the issues of specific interactions and chain dynamics in a systematic fashion.

Acknowledgment. We are indebted to the National Science Foundation for continued support of our program through Grant No. CHE-0518300 and instrumentation Grant No. CHE-9709037. This work received partial support from the STC Program of the National Science Foundation under Agreement No. CHE-9876674.

References and Notes

(1) *Innovations in Supercritical Fluids: Science and Technology*; Hutchenson, K. W., Foster, N. R., Eds.; ACS Symposium Series 608; American Chemical Society: Washington, DC, 1994. McHugh, M. A.; Krukonis, V. J. *Supercritical Fluid Extraction*; Butterworth-Heinemann: Boston, 1994.

(2) (a) Jones, C. A.; Geissler, A.; DeYoung, J. P.; McClain, J. B.; Carbonell, R.; DeSimone, J. M. *Crit. Rev. Solid State Mater. Sci.* **2004**, *29*, 97−109. (b) Hoggan, E. N.; Flowers, D.; Wang, K.; DeSimone, J. M.; Carbonell, R. G. *Ind. Eng. Chem. Res.* **2004**, *43*, 2113.

(3) (a) DeSimone, J. M.; Maury, E. E.; Menceloglu, Y. Z.; McClain, J. B.; Romack, T. J.; Combes, J. R. *Science* **1994**, *265*, 356. (b) Clark, M. R.; DeSimone, J. M. *Macromolecules* **1995**, *28*, 3002. (c) Kapellen, K. K.; Mistele, C. D.; DeSimone, J. M. *Macromolecules* **1996**, *29*, 495.

(4) DeSimone, J. M.; Guan, Z.; Elsbernd, C. S. *Science* **1992**, *257*, 945.

(5) (a) Bunyard, W. C.; Romack, T. J.; DeSimone, J. M. *Macromolecules* **1999**, *32*, 8224. (b) Quadir, M. A.; DeSimone, J. M.; van Herk, A. M.; German, A. L. *Macromolecules* **1998**, *31*, 6481. (c) Ye, W.; DeSimone, J. M. *Ind. Eng. Chem. Res.* **2000**, *39*, 4564. (d) *Green Chemistry Using Liquid and Supercritical Carbon Dioxide*; DeSimone J. M., Tumas, W., Eds.; Oxford University Press: New York, 2003. (e) Kimura, Y.; Kanda, D.; Terazima, M.; Hirota, N. *J. Phys. Chem. B* **1997**, *101*, 4442.

(6) (a) Lacroix-Desmazes, P.; André, P.; DeSimone, J. M.; Ruzette, A.; Boutevin, B. *J. Polym. Sci., Part A: Polym. Chem.* **2004**, *42*, 3537. (b) Roberts, C. B.; Chateauneuf, J. E.; Brennecke, J. F. *J. Am. Chem. Soc.* **1992**, *114*, 8455. (c) Sun, Y.-P.; Fox, M. A.; Johnston, K. P. *J. Am. Chem. Soc.* **1992**, *114*, 1187. (d) Inomata, H.; Hamatani, H.; Wada, N.; Yagi, Y.; Saito, S. *J. Phys. Chem.* **1993**, *97*, 6332.

(7) (a) Randolph, T. W.; Blanch, H. W.; Prausnitz, J. M. *AIChE J.* **1988**, *34*, 1354. (b) Randolph, T. W.; Carlier, C. *J. Phys. Chem.* **1992**, *96*, 5146.

(8) Dukes, K. E.; Harbron, E. J.; Forbes, M. D. E.; DeSimone, J. M. *Rev. Sci. Instrum.* **1997** *68*, 2505.

(9) (a) Closs, G. L.; Forbes, M. D. E. *J. Am. Chem. Soc.* **1987**, *109*, 6185. (b) Closs, G. L.; Forbes, M. D. E. In *Kinetics and Spectroscopy of Carbenes and Biradicals*; Platz, M., Ed.; Plenum: New York, 1990; pp 51−75. (c) Closs, G. L.; Forbes, M. D. E. *J. Phys. Chem.* **1991**, *95*, 1924.

(10) (a) Forbes, M. D. E. *J. Phys. Chem.* **1993**, *97*, 3390. (b) Forbes, M. D. E. *J. Phys. Chem.* **1993**, *97*, 3396.

(11) Forbes, M. D. E.; Ruberu, S. R. *J. Phys. Chem.* **1993**, *97*, 13223.

(12) Forbes, M. D. E.; Ball, J. D.; Avdievich, N. I. *J. Am. Chem. Soc.* **1996**, *118*, 4707.

(13) Forbes, M. D. E.; Closs, G. L.; Calle, P.; Gautam, P. *J. Phys. Chem.* **1993**, *97*, 3384.

(14) (a) Hudson, A.; Luckhurst, G. R. *Chem. Rev.* **1969**, *69*, 191. (b) Shultz, D. A.; Boal, A. K.; Lee, H.; Farmer, G. T. *J. Org. Chem.* **1999**, *64*, 4386.

(15) (a) Shultz, D. A.; Boal, A. K.; Farmer, G. T. *J. Org. Chem.* **1998**, *63*, 9462. (b) Shultz, D. A.; Lee, H.; Fico, R. M., Jr. *Tetrahedron* **1999**, *55*, 12079.

(16) Forbes, M. D. E. *Photochem. Photobiol.* **1997**, *65*, 73.

(17) Harbron, E. J.; Forbes, M. D. E. *Encycl. Chem. Phys. Phys. Chem.* **2001**, *2*, 1389.

(18) (a) Closs, G. L.; Forbes, M. D. E.; Norris, J. R., Jr. *J. Phys. Chem.* **1987**, *91*, 3592. (b) Buckley, C. D.; Hunter, D. A.; Hore, P. J.; McLauchlan, K. A. *Chem. Phys. Lett.* **1987**, *135*, 307. (c) Ishawata, N.; Murai, H.; Kuwata, K. *Res. Chem. Int.* **1993**, *19*, 59. (d) Tarasov, V. F.; Bagranskaya, E. G.; Shkrob, I. A.; Avdievich, N. I.; Ghatlia, N. D.; Lukzen, N. N.; Turro, N. J.; Sagdeev, R. Z. *J. Am. Chem. Soc.* **1995**, *117*, 110. (e) Weis, V.; Van Willigen, H. *J. Porphyrins Phthalocyanines* **1998**, *2*, 353. (f) Bittl, R.; Schulten, K. *J. Chem. Phys.* **1986**, *84*, 9. (g) Bittl, R.; Schulten, K. *Chem. Phys. Lett.* **1988**, *146*, 58. (h) Lebedeva, N. V.; Bagryanskaya, E. G.; Koptyug, I. V.; Sagdeev, R. Z.; Forbes M. D. E. *Chem. Phys. Lett.* **1999**, *308*, 295.

(19) Tarasov, V. F.; Forbes, M. D. E. *Spectrochim. Acta, Part A* **2000**, *56*, 245.

(20) (a) Shushin, A. I. *Chem. Phys. Lett.* **1995**, *245*, 183. (b) Shushin, A. I. *Chem. Phys. Lett.* **1997**, *275*, 137. (c) Shushin, A. I. *Chem. Phys. Lett.* **1998**, *282*, 413. (d) Hore, P. J.; Hunter, D. A. *Mol. Phys.* **1992**, *75*, 1401. (e) Shushin, A. I. *J. Chem. Phys.* **1994**, *101*, 8747. (f) Shushin, A. I. *Chem. Phys. Lett.* **1991**, *177*, 338. (g) Adrian, F. J. *J. Chem. Phys.* **1995**, *102*, 4409. (h) Neufeld A. A.; Pedersen, J. B. *J. Chem. Phys.* **1998**, *109*, 8743. (i) Neufeld A. A.; Pedersen, J. B. *J. Chem. Phys.* **2000**, *113*, 1595.

(21) (a) Avdievich, N. I.; Forbes, M. D. E. *J. Phys. Chem.* **1995**, *99*, 9660. (b) Avdievich, N. I.; Forbes, M. D. E. *J. Phys. Chem.* **1996**, *100*, 1993.

(22) (a) Forbes, M. D. E.; Schulz, G. R.; Avdievich, N. I. *J. Am. Chem. Soc.* **1996**, *118*, 10652. (b) Forbes, M. D. E.; Avdievich, N. I.; Schulz, G. R.; Ball, J. D. *J. Phys. Chem.* **1996**, *100*, 13887.

(23) (a) Tsentalovich Y. P.; Forbes, M. D. E. *Mol. Phys.* **2002**, *100*, 1209. (b) Tsentalovich, Y. P.; Forbes, M. D. E.; Morozova, O. B.; Plotnikov, I. A.; McCaffrey, V. P.; Yurkovskaya, A. V. *J. Phys. Chem. A* **2002**, *106*, 7121.

(24) Tsentalovich, Yu. P.; Fischer, H. *J. Chem. Soc., Perkin Trans. 2* **1994**, 729.

(25) Makarov, T. N.; Bagryanskaya, E. G.; Paul, H. *Appl. Magn. Res.* **2004**, *26*, 1.

(26) Yurkovskaya, A. V.; Galimov, R. R.; Obynochny, A. A.; Salikhov, K. M.; Sagdeev, R. Z. *Chem. Phys.* **1987**, *112*, 259.

(27) De Kanter, F. J. J.; den Hollander, J. A.; Huizer, A. H.; Kaptein, R. *Mol. Phys.* **1977**, *34*, 857.

(28) For discussions of small molecule solubility in CO_2, see: (a) Ikushima, Y.; Saito, N.; Arai, M. *J. Phys. Chem.* **1992**, *96*, 2293. (b) Politzer, P.; Murray, J. S.; Lane, P.; Brinck, T. *J. Phys. Chem.* **1993**, *97*, 729. (c) Souvignet, I.; Olesik S. V. *J. Phys. Chem.* **1995**, *99*, 16800.

(29) Hoefling, T. A.; Enick, R. M.; Beckman, E. J. *J. Phys. Chem.* **1991**, *95*, 7127.

(30) (a) Kumar, K.; Waldeck, D. H.; Zimmt, M. B. *J. Am. Chem. Soc.* **1996**, *118*, 243. (b) Cave, R. J.; Newton, M. D.; Kumar, K.; Zimmt, M. B. *J. Phys. Chem.* **1995**, *99*, 17501. (c) Paddon-Row, M. N.; Shephard, M. J.; Jordan, K. D. *J. Phys. Chem.* **1993**, *97*, 1743.

(31) Kazarian, S. G.; Vincent, M. F.; Bright, F. V.; Liotta, C. L.; Eckert, C. A. *J. Am. Chem. Soc.* **1996**, *118*, 1729.

(32) Dardin, A.; DeSimone, J. M.; Samulski, E. T. *J. Phys. Chem. B* **1998**, *102*, 1775.

(33) Cece, A.; Jureller, S. H.; Kerschner, J. L.; Moschner, K. F. *J. Phys. Chem.* **1996**, *100*, 7435.

(34) Han, Y.-K.; Jeong, H. Y. *J. Phys. Chem. A* **1997**, *101*, 5604.